UDC 621.314 https://doi.org/10.20998/2074-272X.2025.2.06

K. Sabhi, M. Talea, H. Bahri, S. Dani

Integrating dual active bridge DC-DC converters: a novel energy management approach for hybrid renewable energy systems

Introduction. *Hybrid renewable energy systems, which integrate wind turbines, solar PV panels, and battery storage, are essential for sustainable energy solutions. However, managing the energy flow in these systems, especially under varying load demands and climatic conditions, remains a challenge. The* ***novelty*** *of this paper is introduces a hybrid renewable energy system structure using Dual Active Bridge (DAB) DC-DC converters and an energy management strategy (EMS) to control power flow more effectively. The approach includes a dump load mechanism to handle excess energy, offering a more efficient and flexible system operation. The* ***purpose*** *of this study is to develop a novel approach to managing and controlling hybrid renewable energy systems, specifically through the use of a DAB DC-DC converter. Unlike traditional methods that may struggle with efficiency and flexibility, our approach introduces an innovative EMS that leverages a reduced neural network block for real-time optimal power tracking and a sophisticated control system to adapt to dynamic conditions. This approach aims to improve the flexibility of the system, enhance energy utilization, and address the limitations of existing methods by ensuring rapid and efficient responses to changes in load and climatic conditions. The primary goal of this study is to improve the performance and reliability of hybrid renewable energy systems by optimizing energy distribution and battery management. The strategy aims to ensure continuous energy availability, enhance battery lifespan, and improve system response to dynamic changes.* ***Methods.*** *The proposed EMS was developed and tested using MATLAB/Simulink. The system's control mechanism prioritizes battery charging when renewable energy output exceeds demand and redirects excess energy to a dump load when necessary. Simulations were conducted under various load and climatic conditions to assess system performance.* ***Results.*** *The simulation results demonstrate that the proposed strategy effectively manages energy flow, ensuring optimal power distribution, quick adaptation to load changes, and maintaining the battery's state of charge within safe limits.* ***Practical value****. The system showed improved stability and efficiency, validating the effectiveness of the control strategy in enhancing the overall performance of hybrid renewable energy systems.* References 33, tables 3, figures 13.

Key words: **hybrid renewable energy system, dual active bridge DC-DC converter, energy management strategy, maximum power point tracking.**

Вступ*. Гібридні системи відновлюваної енергетики, які об'єднують вітряні турбіни, сонячні фотоелектричні панелі та акумуляторні батареї, є важливими для стійких енергетичних рішень. Однак управління потоком енергії в цих системах, особливо за змінних вимог до навантаження та кліматичних умов, залишається проблемою.* ***Новизна*** *цієї статті полягає в представленні гібридної структури системи відновлюваної енергії з використанням подвійних активних мостів (DAB) DC-DC перетворювачів і стратегії управління енергією (EMS) для більш ефективного контролю потоку електроенергії. Цей підхід включає механізм скидання навантаження для обробки надлишкової енергії, що забезпечує більш ефективну та гнучку роботу системи.* ***Метою*** *цього дослідження є розробка нового підходу до управління та контролю гібридних систем відновлюваної енергії, зокрема за допомогою перетворювача DAB DC-DC. На відміну від традиційних методів, які можуть мати проблеми з ефективністю та гнучкістю, наш підхід запроваджує інноваційну EMS, яка використовує зменшений блок нейронної мережі для відстеження оптимальної потужності в реальному часі та складну систему керування для адаптації до динамічних умов. Цей підхід спрямований на покращення гнучкості системи, покращення використання енергії та усунення обмежень існуючих методів шляхом забезпечення швидкої та ефективної реакції на зміни навантаження та кліматичних умов. Основною метою цього дослідження є покращення продуктивності та надійності гібридних систем відновлюваної енергії шляхом оптимізації розподілу енергії та керування батареями. Стратегія спрямована на забезпечення безперервної доступності енергії, збільшення терміну служби акумулятора та покращення реакції системи на динамічні зміни.* ***Методи****. Запропонована EMS була розроблена та протестована за допомогою MATLAB/Simulink. Механізм керування системою надає пріоритет зарядці батареї, коли вихід відновлюваної енергії перевищує попит, і за необхідності перенаправляє надлишкову енергію на скидання. Для оцінки продуктивності системи було проведено моделювання за різних навантажень і кліматичних умов.* ***Результати*** *моделювання демонструють, що запропонована стратегія ефективно керує потоком енергії, забезпечуючи оптимальний розподіл потужності, швидку адаптацію до змін навантаження та підтримку стану заряду батареї в безпечних межах.* ***Практична значимість****. Система продемонструвала покращену стабільність та ефективність, підтверджуючи ефективність стратегії керування для підвищення загальної продуктивності гібридних систем відновлюваної енергії.* Бібл. 33, табл. 3, рис. 13.

Ключові слова: **гібридна система відновлюваної енергії, подвійний активний мостовий DC-DC перетворювач, стратегія управління енергією, відстеження точки максимальної потужності.**

Introduction. Renewable energy sources (RESs) are gaining increasing attention as a sustainable alternative to traditional fossil fuels, which have negative environmental impacts and limited availability. Various RESs, such as solar, wind, and hydropower, have been developed to harness clean and abundant energy from natural resources [1–5]. However, single source renewable energy systems have several limitations, such as intermittency, variability, and low efficiency. To overcome these limitations, hybrid renewable energy system (HRES) is an effective solution [6–8].

HRESs combine two or more RESs to improve the system's reliability, stability, and performance [9–11]. These systems can be configured in various ways, depending on the available RESs, system requirements, and design constraints. The most common configurations include PV/wind hybrid systems [9], PV/hydropower hybrid systems, and wind/fuel cell hybrid systems [6].

Several studies have been conducted to evaluate the performance and efficiency of different HRESs. These studies employ various methodologies, including simulation, optimization and experimental analysis [10].

In recent years, significant progress has been made in the field of HRESs, with numerous studies reporting successful implementation of these systems in various applications, such as rural electrification, microgrids and building integration [11]. However, challenges such as cost-effectiveness, scalability, and reliability still need to be addressed to facilitate the widespread adoption of HRESs [12].

In the literature we can distinguish several structures of hybrid systems based on renewable energies, there are two more useful types of hybrid system structures, specifically the DC bus structure [1–12] and the multiport converter structure [13], irrespective of their operating mode, standalone and grid-connected mode.

HRES based on ordinary DC-DC converters is a configuration that combines various RESs, including solar panels, wind turbines (WTs) and batteries [14], integrating them into a shared DC bus. This approach involves converting the energy generated by these sources into DC and merging them into a unified bus, enabling efficient energy management and optimal resource utilization [15].

Another approach looks at the implementation of a new secondary structure designed to streamline protection measures, minimizing the need for protection circuits. Another advantage of this type of structure is to ensure galvanic isolation without additional circuits [16], thereby enhancing safety and reducing electromagnetic interference.

This research embarks on a comprehensive exploration of a specific HRES configuration, strategically integrating solar panels, WT, a load and a dump load. At the heart of this integration is a battery storage system, the latter is connected to the other elements by a DC-DC Dual Active Bridge (DAB) converter, a technological cornerstone streamlining the interconnection of various energy sources [17–19]. The DAB converter, equipped with a single-phase high-frequency transformer, also strengthens the system against voltage fluctuations and other operational challenges.

The orchestration of this energetic symphony relies largely on a sophisticated control strategy. The crux of this strategy lies in the manipulation of the phase shift within each transformer. This control ensures optimal contributions from each energy source to interconnected loads, aligning with constantly fluctuating power demands. The battery storage system, the central element of this arrangement, seamlessly transitions between charging and discharging modes, acting as a stabilizing force that mitigates the impact of intermittent renewable sources.

The impact of climatic conditions on power availability is uncertain; the operating point often changes, to control the latter the DABs are controlled by a PI regulator, whose reference is precomputed by a reduced neural network block and a structural approximation which makes it possible to extract the maximum power point (MPP) of photovoltaic (PV) array [20] and WT energy [21].

The goal of the paper is to enhance the flexibility and efficiency of HRESs by developing an advanced control strategy. This approach aims to improve the adaptability of the system's structure and streamline the management of currents supplied or consumed by different components. The paper introduces a novel method for optimizing the use of RESs, utilizing a reduced neural network block for precise reference calculation. It focuses on effective energy management based on the State of Charge (SOC) of the battery and the load requirements. The proposed strategy ensures a rapid and adaptive response to load fluctuations, sudden changes in climatic conditions, and variations in energy availability. Performance evaluation is conducted through simulations using MATLAB/Simulink, with results compared to existing control strategies and management approaches.

System performance is simulated using the MATLAB/Simulink software; results were compared to the control approach to management organization charts.

System description. This paper carries out a HRES, depicted in Fig. 1, comprises a permanent magnet synchronous generator (PMSG) WT, solar PV panels, a variable load, and a dump load, these components are interconnected with a battery energy storage system each through a DAB DC-DC converter [19].

With the PV panel as the first input, the PMSG WT as the second input, the third input linked to the load, the fourth is gave to the dump load and the common and the fifth designated for the battery. The system operates independently in standalone mode.

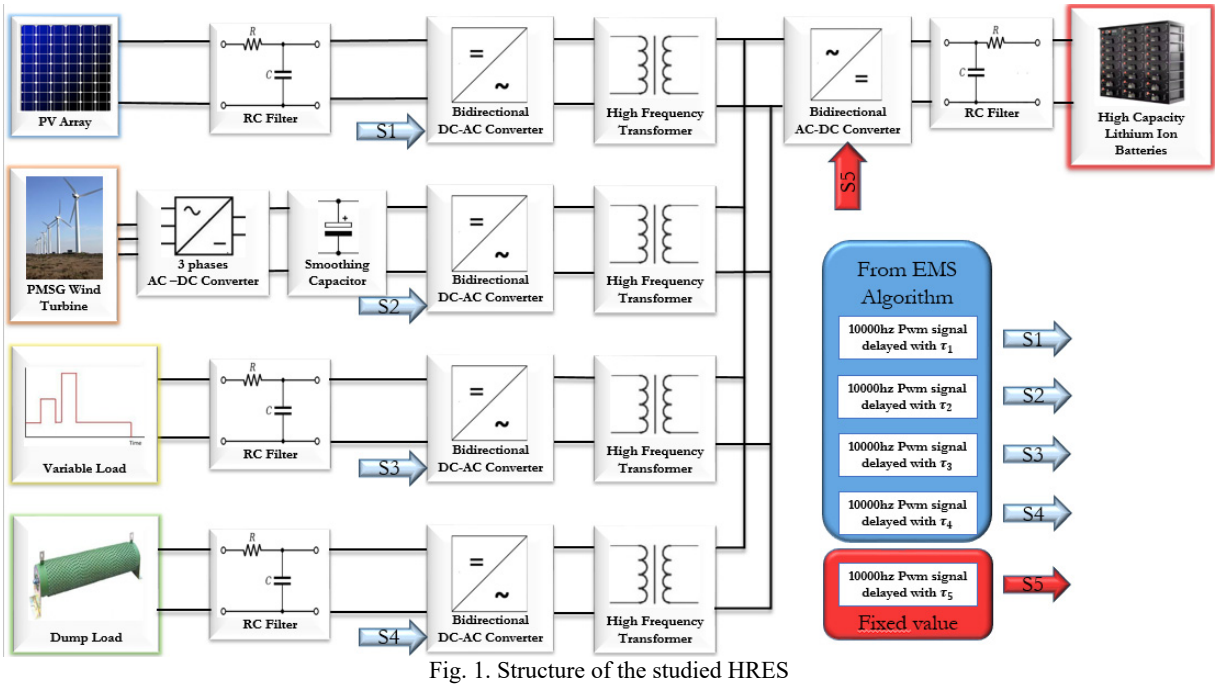

Fig. 1. Structure of the studied HRES

To regulate both the quantity and direction of power transfer, the rectangular waveforms generated exhibit controlled phase shifts with respect to each other. The relative delays, namely τ_{15} (controlling power flow from PV to the battery), τ_{25} (for power flow from the WT to the battery), τ_{35} (variable load to the battery) and τ_{45} (dump load to the battery), τ_{jk} determine the extent of phase shift. Positive values of indicate that the voltage in port j is leading the reference voltage in port k, while negative values imply the opposite.

The proposed energy management system is illustrated in Fig. 2 as a block diagram, showing its inputs and outputs. The management method in this study relies

on several key elements: it prioritizes charging the batteries when the load demand exceeds what the RESs can supply and pass the excess of power through a fixed dump resistor when the battery is maximally charged. This approach ensures the continuous availability of energy, extends the battery life cycle, and improves system efficiency.

Fig. 2. Block diagram of the energy management system

Modeling and sizing of electrical system parameters.

1. PV source. PV cell's equivalent diagram (Fig. 3) features a generator current that simulates illumination and a parallel diode representing the PN junction. The practical circuit also takes into account parasitic resistive effects due to manufacturing [22, 23].

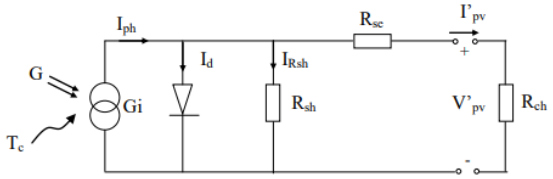

Fig. 3. Equivalent diagram of a PV cell

The solar PV module is formed by connecting PV cells in both series and parallel configurations. The current output I_{pv} from the solar PV module is determined as:

$$I_{pv} = N_p(I_{ph} - I_d e^{\left(\frac{qV_d}{N_s AkT}\right)} - 1) - \frac{V_d}{R_{sh}}, \quad (1)$$

where N_p is the number of cells in parallel; N_s is the number of cells in series; I_{ph} is the photocurrent; I_d is the reverse saturation current; V_d is the diode voltage; A is the diode ideality factor; k is the Boltzmann's constant; T is the temperature; q is the elementary charge; R_{sh} is associated with the non-ideal characteristics of the p-n junction and the presence of defects along the cell's edges that create a short-circuit path around the junction; R_{se} is the overall resistance encountered by the electrons along their path.

PV array used in this study under standard testing conditions of solar irradiance G = 1000 W/m² and a temperature of T = 25 °C (Table 1).

Table 1

Specification of the PV

Parameter	Value
Maximum power of the solar panel P_{mpp}, kW	64
Current at MPP I_{mpp}, A	110.25
Voltage at the MPP V_{mpp}, V	580
Short-circuit current I_{sc}, A	117.6
Open circuit voltage value V_{0cs}, V	726

2. WT model. Numerous mathematical models have been developed to describe the relationship between wind speed and the mechanical power generated from wind. In this study, the WT is represented as [24]:

$$P_w = \frac{1}{2}\rho A_r C_p v^3, \quad (2)$$

where P_w is the wind power extracted; ρ is the air density; A_r is the rotor area of the WT; v is the wind speed; C_p is the power coefficient. The power coefficient is influenced by the tip speed ratio λ and the pitch angle β.

Numerical approximations are utilized to compute C_p for specified values of λ and β, as shown in [24] with the following expression:

$$C_p(\lambda,\beta) = c_1\left(\frac{c_2}{\lambda_i} - c_3\beta - c_4\right)e^{-\frac{c_5}{\lambda_i}} + c_6\lambda; \quad (3)$$

$$\lambda_i = \left[\left(\frac{1}{\lambda + 0.08\beta}\right) - \left(\frac{0.035}{\beta^3 + 1}\right)\right]^{-1}. \quad (4)$$

The coefficient C_p utilized for the simulation, as referenced in [25], are: c_1=0.5176, c_2=116, c_3=0.4, c_4=5, c_5=21, c_6=0.0068. Notably, the maximum C_p ($C_{p\max}$) is achieved at an optimal tip speed ratio (λ_{opt}) and a pitch angle of β = 0. Additionally, a relationship linking the rotor speed to the tip speed ratio [3] is expressed as:

$$\lambda = \frac{\omega_r \cdot R}{v}, \quad (5)$$

where R is the length of the WT blade.

The characteristics of the WT at V = 12 m/s and β=0 used are presented in Table 2.

Table 2

WT specification

Parameter	Value
Maximal power P_{mpp}, kW	100
Density of air ρ, kg/m^3	1.12
Radius of rotor R, m	8.28
Turbine total inertia, kg·m^2	0.1
Total viscous friction, N·s/m^2	0.0004924

3. Dual active bridge. Figure 4 shows a typical full-bridge DAB DC/DC converter that interfaces between two voltage sources and its equivalent circuit. The two actively controlled full bridges are connected via a high-frequency transformer [26]. The power inductor L_s, which includes the leakage inductance, serves as the main energy transfer device.

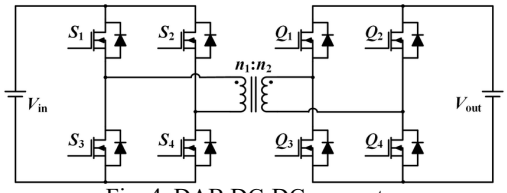

Fig. 4. DAB DC-DC converter

DAB converter is characterized by its easy control, high efficiency, high power density and galvanic isolation ensures by the transformer.

The power transfer between the two windings, represented as P_{jk}, is regulated using a simple-phase-shift technique [27]. This relationship is described by the following equation, while admitting that n_1=n_2:

$$P_{jk} = \frac{V_j V_k D_{jk}(1-|D_{jk}|)}{2 f_s L_{jk}}; \quad |D_{jk}| \le 1, \qquad (6)$$

$$D_{jk} = 2\frac{\tau_{jk}}{T_s}; \qquad (7)$$

$$\tau_{jk} = (\tau_k - \tau_j), \qquad (8)$$

where τ_{jk} is the relative delay between the square wave signals from inverters j and k; τ_k and τ_j are the absolute delays of the signals V_k and V_j, respectively; T_s is the period of the square wave signals, also known as the switching period [27].

Assuming the following equality based on (7), (8):

$$D_{jk} = D_k - D_j. \qquad (9)$$

MPPT method. Application on PV generator. This part of the energy management process begins with setting the irradiance G = 1000 W/m². It uses a simplified neural network block that takes temperature T and irradiance G as inputs and provides I_{opt} as the output.

The nntool Toolbox in MATLAB is used for designing, training, validating and testing a neural network. The dataset is divided into 3 parts: 70 % for training, 15 % for validation and 15 % for testing. The neural network is trained using the Levenberg-Marquardt algorithm, which is a very fast and accurate method for minimizing the mean square error (Fig. 5). This algorithm provides superior results compared to others. The regression results are depicted in Fig. 6.

Train a neural network to map predictors to continuous responses.

Data

Predictors: in - [1x61 double]
Responses: inn - [1x61 double]

in: double array of 61 observations with 1 features.
inn: double array of 61 observations with 1 features.

Algorithm

Data division: Random
Training algorithm: Levenberg-Marquardt
Performance: Mean squared error

Training Results

Training start time: 30-Jul-2024 20:24:43
Layer size: 10

	Observations	MSE	R
Training	43	0.0127	0.9947
Validation	9	0.0059	0.9969
Test	9	0.0109	0.9975

Fig. 5. ANN model summary

In the second step, an adaptation block is developed to calculate I_{opt} for any irradiance level by referencing the value obtained at 1000 W/m². We will validate this adaptation with experimental results.

The idea stems from the observed proportionality in the PV graphs at a constant temperature. Using the case presented in Table 3, for a fixed temperature T = 25°C, we compare the relative value G/1000 with I_{opt}/I_{opt}(1000) for irradiances ranging from 100 to 1000. According to the neural network block at T = 25°C, I_{opt}(1000) = 110 A.

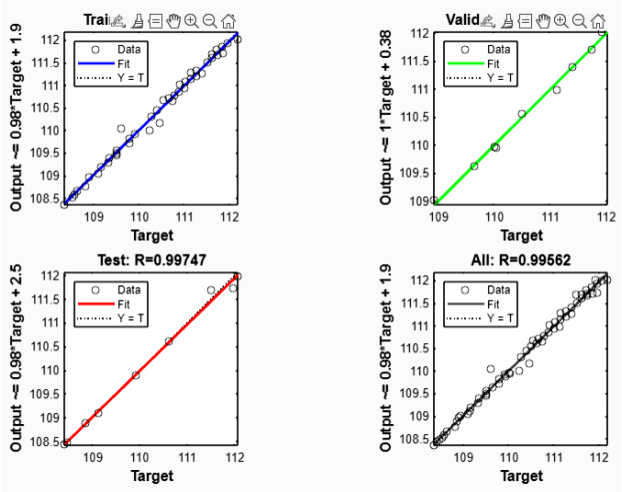

Fig. 6. The regression results

Table 3 demonstrates the approximate equality of G/1000 and $I_{opt}(G)/I_{opt}$(1000). Therefore, the adaptation we adopted involves first determining I_{opt} at any temperature for G = 1000 W/m² and then multiplying it by G/1000. The effectiveness of this technique will be validated in the results discussion section.

Table 3

Optimal current I_{opt} at different irradiance values G and T = 25°C

G	G/1000	I_{opt}	I_{opt} / I_{opt}(1000)
100	0.1	11.07	0.10063636363
200	0.2	22.155	0,20140909090
300	0.3	33.1763	0,30160272727
400	0.4	44.226	0,40205454545
500	0.5	55.2232	0,50202909090
600	0.6	66.2241	0,60203727272
700	0.7	77.2974	0,70270363636
800	0.8	88.2805	0,80255000000
900	0.9	99.6837	0,90621545454
1000	1	110	1

Figure 7 shows the circuit configuration between the PV and the battery this kind of techniques is represented in [28–32].

The energy management system is a computerized system, which allows, firstly, to find the current instructions to extract the maximum power from RESs, while referring to the SoC of the battery and secondly a regulation system which makes it possible to control the three converters in order to guarantee the performance of the powers in each element of our system.

The flowchart shown in Fig. 8 deploys the energy management strategy (EMS) proposed by our work. The management algorithm is designed to adjust the 4 phase shifts based on the reference, which is the battery, as mentioned in the system description. These adjustments are driven by 2 key factors: SOC of the battery and the comparison between the power demanded by the load and the power supplied in real time by the RESs.

The algorithm presented in Fig. 8 is summarized in the following situations:

1. Situation 1. When the total power produced by RESs is less than the power demanded by the load, and

SoC is greater than 85 %, the battery discharges and contributes to meeting the demand.

2. Situation 2. In this case, if SoC of the battery is greater than 85 % and the load demand is lower than the production from the RES, the battery is isolated, and the excess power produced is directed towards the dump load.

3. Situation 3. In this situation [33], if the SoC is between 15 % and 85 % and the power produced by the RES is lower than the load demand, the battery discharges to cover the remaining demand.

4. Situation 4. When the load demand is lower than the power produced by the RESs and the battery's SoC is between 15 % and 85 % [33], the excess power is directed to the battery, indicating that the battery is charging.

5. Situation 5. If the SoC is now less than 15 % and the power from the RESs exceeds the demand, the battery will be charged by the excess power.

6. Situation 6. The last situation involves isolating the load while the battery is charging when the battery's SoC is below 15 % and the RES cannot meet the load demand.

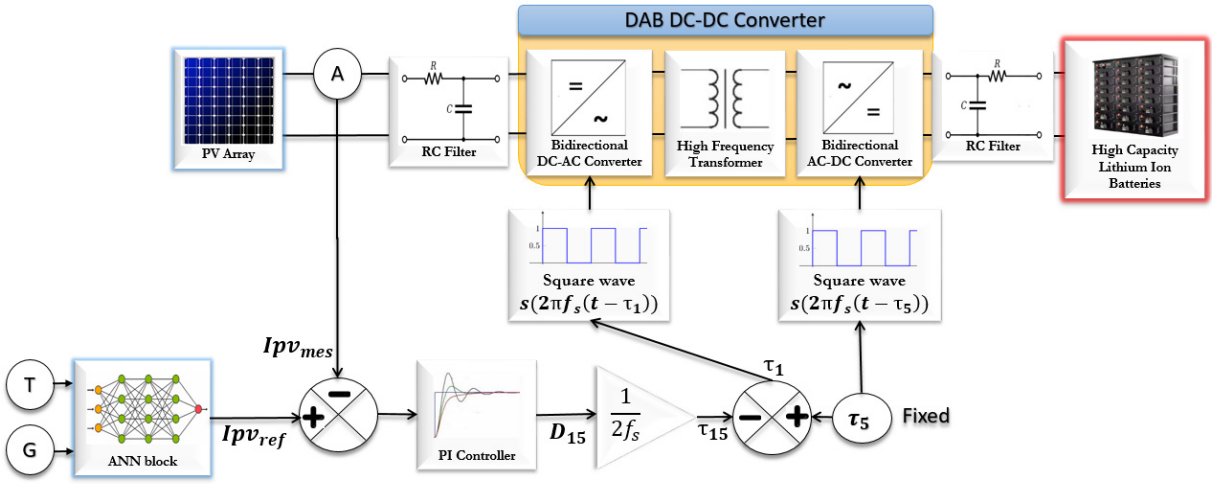

Fig. 7. Proposed MPPT control diagram block

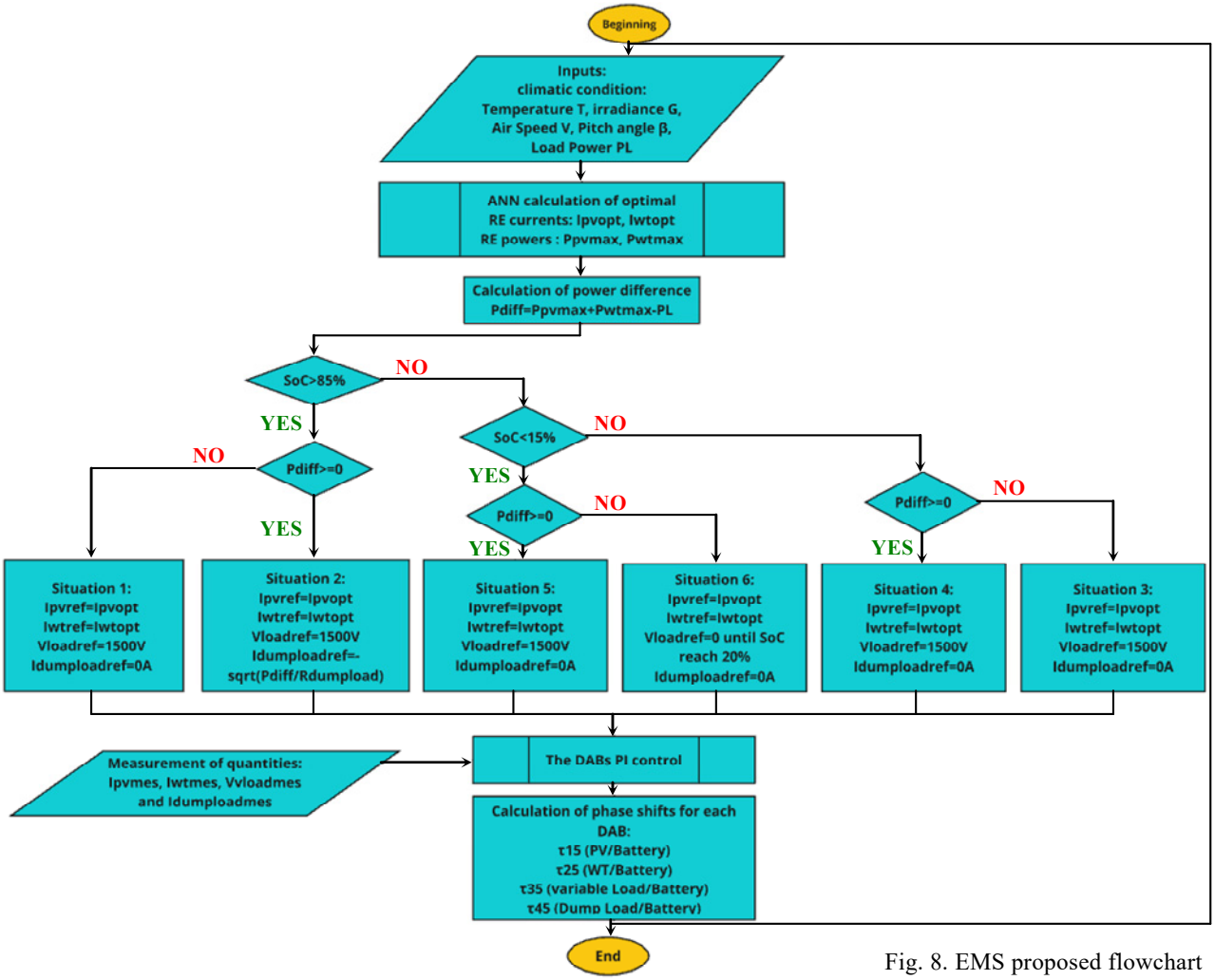

Fig. 8. EMS proposed flowchart

Results and discussion.

1. MPPT method validation. The test presented in Fig. 9,*a* assesses the reliability and capability of our control system to track maximum power. As previously mentioned, the optimal current under specific climatic conditions is calculated using a simplified neural network block and an adaptation method.

In this scenario, the PV system is subjected to a temperature $T = 30$°C and an irradiance $G = 850$ W/m².

The block provided 94 A as the reference current. To verify the block's reliability, we applied 3 reference currents to the PI regulation system with a 0.6 s delay: initially 94.5 A, then 94 A at 0.2 s (as calculated by the block), and finally 93.5 A at 0.4 s. The average power at the PV level was evaluated for the 3 cases. Figure 9,*b* summarizes these results.

After analyzing the residual graph, we see that the regulation system accurately followed the current references. For each current, the PV system developed an average power: approximately 53540 W for 94.5 A, 53552 W for 94 A (as calculated by the block), and 53539 W for 93.5 A. These results indicate that our system achieved maximum power for the reference calculated by our block, demonstrating that the MPPT approach is both efficient and reliable. It is worth noting that the system produced consistent results under different climatic conditions, which should be considered in the optimization algorithm.

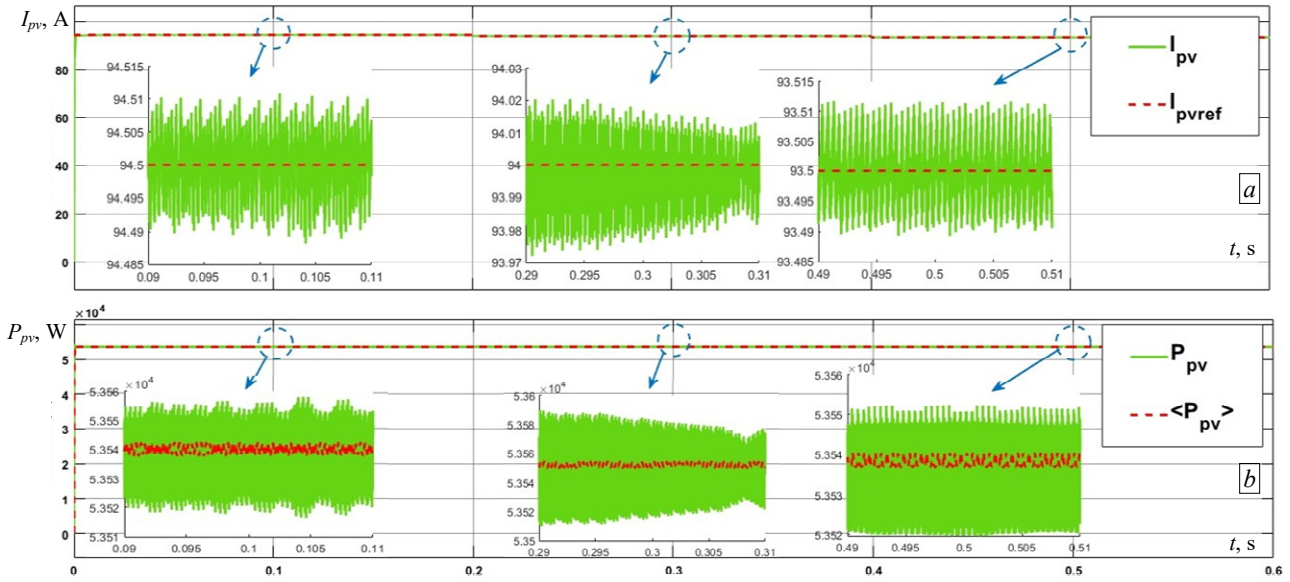

Fig. 9. MPPT PV results

2. EMS scenarios. In this section, we will evaluate the developed algorithm under different scenarios. One important thing to consider is that we did not vary the climatic conditions of the WT.

In a 4-second simulation, we evaluated the system's performance across the first 4 situations by adjusting the irradiation G, temperature T and changing the load demand. The results are presented in Fig. 9, 10.

Regarding the load, it requires 125 kW between 0 and 2 s, and 186.5 kW between 2 s and 4 s.

Between 0 and 1.33 s, the PV system operated at a temperature of 22 °C and an irradiance of 600 W/m², producing 39,32 kW. From 1.33 s to 2.66 s, with the temperature at 27 °C and irradiance at 1000 W/m², the power output increased to 63,35 kW. Finally, between 2.66 s and 4 s, at 25 °C and 900 W/m², the PV system generated 57,75 kW.

The climatic conditions for the WT were fixed throughout the simulation, with a wind speed of 12 m/s and a pitch angle of 0°, resulting in an average power output of 98,5 kW.

Based on the data provided, we can conclude that between 0 and 2 s, the power generated by the RESs exceeds the load demand, while between 2 s and 4 s, the opposite is true.

We began with the SoC of 84.9972 % to ensure a smooth transition between situations. Initially, we were in situation 4, which was confirmed by the simulation. At 0.91 s the battery reached 85 % (Fig. 11). At this point, we transitioned to situation 2 by isolating the battery through a command and diverting the excess power to the dump load. In Fig. 10, the dump load is represented by the power P_{dl}.

At 2 s, the SoC is still slightly above 85 %, and as the power demand exceeds production, the system shifts to situation 1. In this scenario, the battery becomes the power source, and the dump load is isolated again. However, this situation only lasts for 0.02 s before the SoC drops below 85 %, moving the system to situation 3, which follows the same instructions as situation 1.

This demonstrates the system's efficiency in regulation and control, as it dynamically adjusts based on the battery's status. For instance, at 2 s (Fig. 10) the load changes its setpoint, yet the system successfully adapts to the new setpoint, while the PV and WT maintain their average values, proving the system's resilience against load disturbances.

To avoid too much repetition, we kept the simulation conditions, including those for the PV, WT, and load, almost the same. This time, we focused on evaluating the energy management system with the SoC around 15 %.

Figure 12 shows the power levels in different situations when the SoC is close to 15 % (Fig. 13).

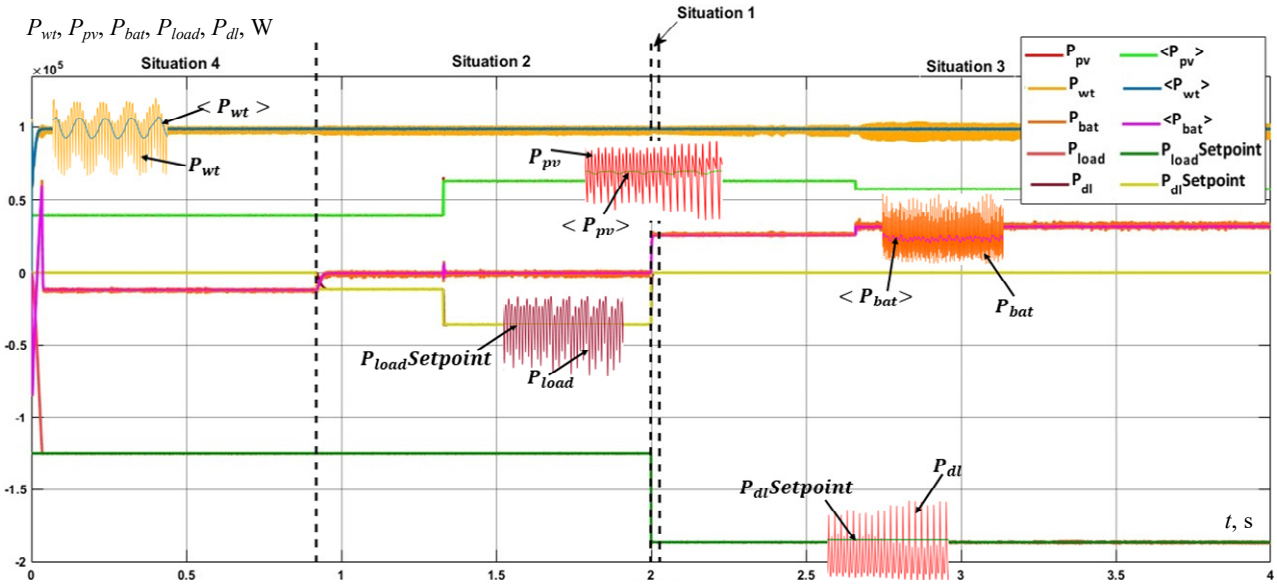

Fig. 10. EMS situations between 1 and 4

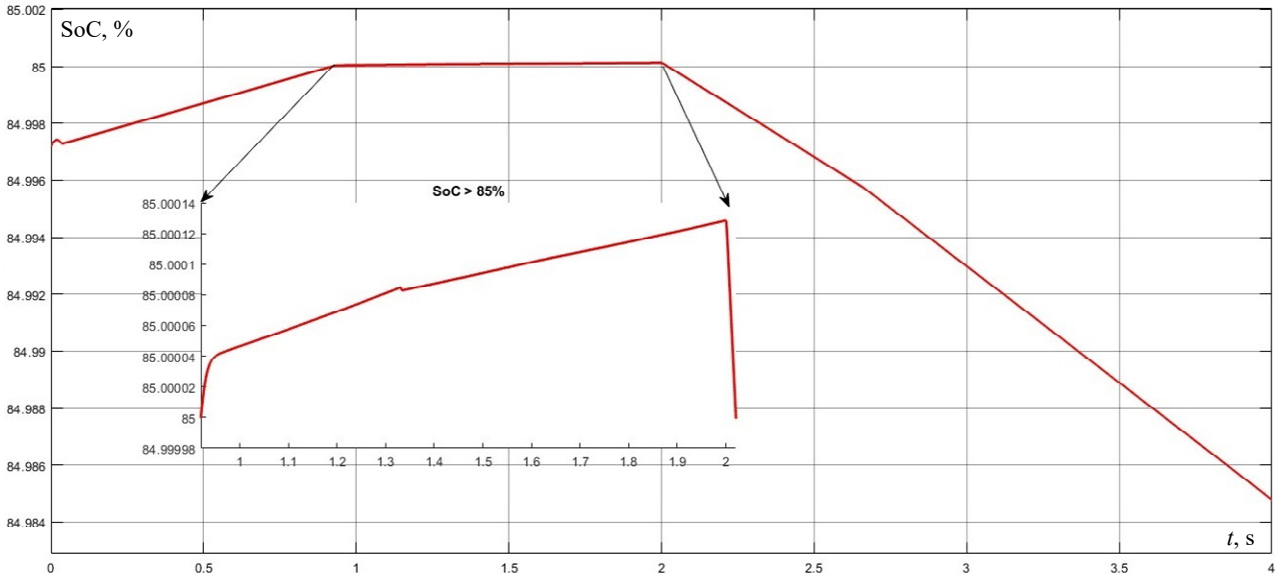

Fig. 11. Battery SOC corresponding situations between 1 and 4

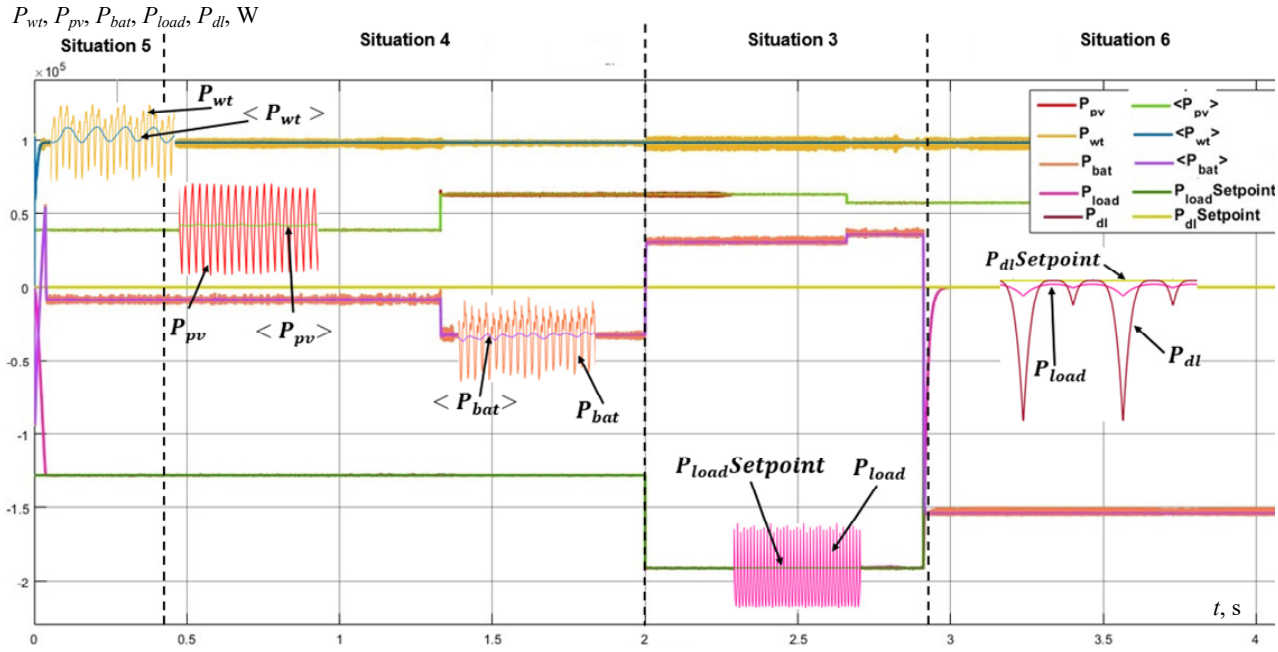

Fig. 12. EMS situations between 3 and 6

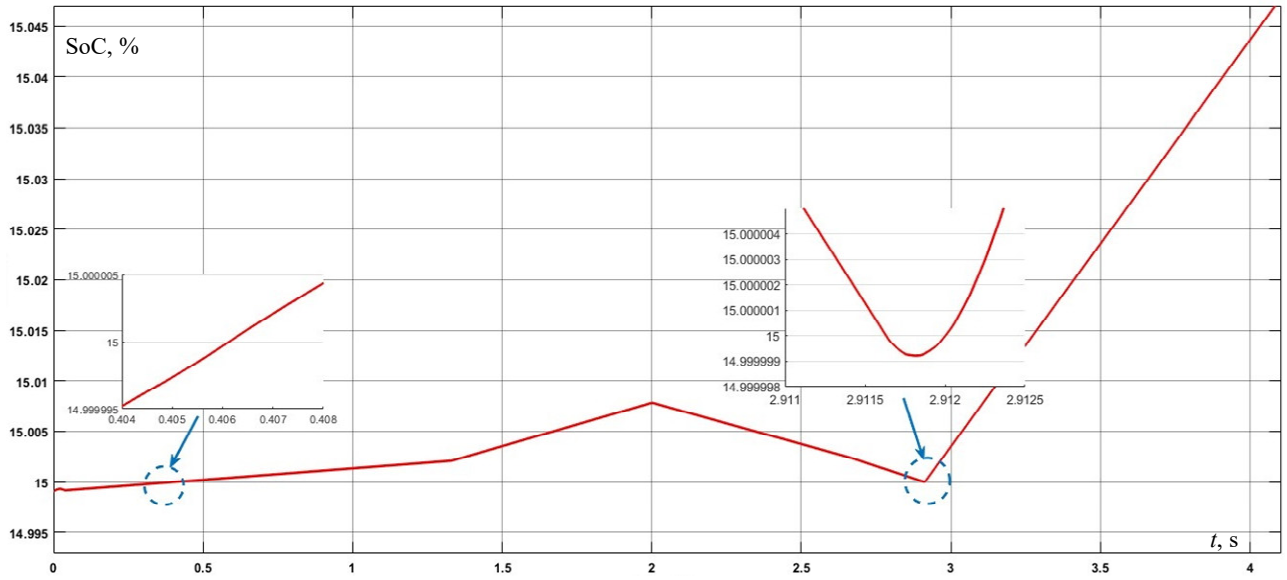

Fig. 13. Battery SOC corresponding situations between 3 and 6

As shown in Fig. 13, the SoC is below 15 % between 0 and 0.406 s. During this time, Fig. 12 indicates that the load's power demand is lower than the combined output of the PV and WT, triggering situation 5. After 0.406 s, the SoC surpasses 15 % under the same conditions, causing a switch to situation 4, which maintains the same outputs as situation 5. The battery continues to charge in this situation until 2 s, when the power demand exceeds what the sources can supply, as long as the SoC remains between 15 % and 85 %, situation 3 is activated, causing the battery to discharge until 2.9115 s, when the SoC reaches 15 %, At this point, a critical situation arises: the battery is at its minimum level, and the load demands more power than is being produced. This triggers situation 6, where charging the battery becomes the priority.

In the scenario shown in Fig. 12, the charging voltage is cut off to allow the battery to charge. To prevent the system from oscillating around 15 % (switching between situations 3 and 6), we implemented a strategy to stabilize the process, we introduce a tolerance band (hysteresis) in SoC levels to avoid frequent switching between charging and discharging modes. In this case, we might wait until SoC rises to 20 % before resuming power to non-critical loads. This prevents short cycling of the battery.

In the scenario shown in Fig. 12, the charging voltage is cut off to allow the battery to charge. To prevent the system from oscillating around 15 % (switching between situations 3 and 6), we implemented a strategy to stabilize the process, we introduce a tolerance band (hysteresis) in SoC levels to avoid frequent switching between charging and discharging modes. In this case, we might wait until the SoC rises to 20 % before resuming power to non-critical loads. This prevents short cycling of the battery.

Conclusions. This research has successfully created and tested a hybrid renewable energy system that combines solar panels, wind turbines, and a battery storage system. The system uses a smart control strategy with a dual active bridge DC-DC converter and an energy management system to effectively manage the energy from different sources and supply it to the load.

One of the main advantages of this system is its flexibility in managing energy. The control strategy adjusts the energy distribution based on changing power demands and environmental conditions, ensuring that all energy sources work together efficiently.

The energy management system is designed to prioritize when to charge or discharge the battery based on its state of charge and the energy demands in real time. This helps to keep the system reliable, extend the battery's lifetime, and improve overall efficiency.

We validated the MPPT method through simulations, showing that it accurately tracks the maximum power available under different weather conditions. The energy management system was also tested under various scenarios, proving its ability to adapt to changes in load and energy generation.

The simulations conducted using MATLAB/Simulink showed that the system performs consistently across different situations. By using a simplified neural network for MPPT and effectively managing the state of charge, the system maintains stable operation and optimizes energy use.

In summary, this hybrid renewable energy system, with its advanced control and management strategies, offers a practical solution for integrating renewable energy sources in a flexible and efficient way. Future research could focus on optimizing the system and on developing other control techniques to further improve the performance of the system.

Conflict of interest. The authors declare that there is no conflict of interest.

REFERENCES

1. Das S., Akella A.K. Power Flow Control of PV-Wind-Battery Hybrid Renewable Energy Systems for Stand-Alone Application. *International Journal of Renewable Energy Research*, 2018, vol. 8, no. 1, pp. 36-43. doi: https://doi.org/10.20508/ijrer.v8i1.6534.g7278.

2. Lu J., Siaw F.L., Thio T.H.G., Wang J.J. Capacity optimization of independent hybrid renewable energy system under different operational strategies based on improved gray wolf algorithm. *AIP Advances*, 2024, vol. 14, no. 5, art. no. 055205. pp. doi: https://doi.org/10.1063/5.0198446.

3. Gajewski P., Pieńkowski K. Control of the Hybrid Renewable Energy System with Wind Turbine, Photovoltaic Panels and Battery Energy Storage. *Energies*, 2021, vol. 14, no. 6, art. no. 1595. doi: https://doi.org/10.3390/en14061595.

4. Vinothkumar J., Thamizhselvan R. Efficient Power Management and Control Strategy of Hybrid Renewable Energy System in Microgrid. *International Journal on Applied Physics and Engineering*, 2023, vol. 2, pp. 106-127. doi: https://doi.org/10.37394/232030.2023.2.11.

5. Jamal S., Pasupuleti J., Ekanayake J. A rule-based energy management system for hybrid renewable energy sources with battery bank optimized by genetic algorithm optimization. *Scientific Reports*, 2024, vol. 14, no. 1, art. no. 4865. doi: https://doi.org/10.1038/s41598-024-54333-0.
6. Ayat Y., Badoud A.E., Mekhilef S., Gassab S. Energy management based on a fuzzy controller of a photovoltaic/fuel cell/Li-ion battery/supercapacitor for unpredictable, fluctuating, high-dynamic three-phase AC load. *Electrical Engineering & Electromechanics*, 2023, no. 3, pp. 66-75. doi: https://doi.org/10.20998/2074-272X.2023.3.10.
7. Bourouis B., Djeghloud H., Benalla H. An innovative algorithm for a hybrid fc/battery system energy management. *Electrical Engineering & Electromechanics*, 2020, no. 6, pp. 35-44. doi: https://doi.org/10.20998/2074-272X.2020.6.06.
8. Tahiri F.E., Chikh K., Khafallah M. Optimal Management Energy System and Control Strategies for Isolated Hybrid Solar-Wind-Battery-Diesel Power System. *Emerging Science Journal*, 2021, vol. 5, no. 2, pp. 111-124. doi: https://doi.org/10.28991/esj-2021-01262.
9. Ndeke C.B., Adonis M., Almaktoof A. Energy management strategy for a hybrid micro-grid system using renewable energy. *Discover Energy*, 2024, vol. 4, no. 1, art. no. 1. doi: https://doi.org/10.1007/s43937-024-00025-9.
10. Iqbal M.M., Kumar S., Lal C., Kumar C. Energy management system for a small-scale microgrid. *Journal of Electrical Systems and Information Technology*, 2022, vol. 9, no. 1, art. no. 5. doi: https://doi.org/10.1186/s43067-022-00046-1.
11. Maaruf M., Khan K., Khalid M. Robust Control for Optimized Islanded and Grid-Connected Operation of Solar/Wind/Battery Hybrid Energy. *Sustainability*, 2022, vol. 14, no. 9, art. no. 5673. doi: https://doi.org/10.3390/su14095673.
12. Cabrane Z., Lee S.H. Control and Management of Railway System Connected to Microgrid Stations. *IEEE Access*, 2022, vol. 10, pp. 40445-40455. doi: https://doi.org/10.1109/ACCESS.2022.3165832.
13. Mechnane F., Drid S., Nait-Said N., Chrifi-Alaoui L. Robust Current Control of a Small-Scale Wind–Photovoltaic Hybrid System Based on the Multiport DC Converter. *Applied Sciences*, 2023, vol. 13, no. 12, art. no. 7047. doi: https://doi.org/10.3390/app13127047.
14. Moghaddam S., Bigdeli M., Moradlou M. Optimal design of an off-grid hybrid renewable energy system considering generation and load uncertainty: the case of Zanjan city, Iran. *SN Applied Sciences*, 2021, vol. 3, no. 8, art. no. 732. doi: https://doi.org/10.1007/s42452-021-04718-x.
15. Menzri F., Boutabba T., Benlaloui I., Khamari D. Optimization of Energy management using a particle swarm optimization for hybrid renewable energy sources. *2022 2nd International Conference on Advanced Electrical Engineering (ICAEE)*, 2022, pp. 1-5. doi: https://doi.org/10.1109/ICAEE53772.2022.9962065.
16. Jafari M., Malekjamshidi Z. A Topology of DC-DC Converter Based on Multi-Winding Transformer for Grid Integration of Multiple Renewable Energy Resources. *Inventions*, 2020, vol. 5, no. 3, art. no. 31. doi: https://doi.org/10.3390/inventions5030031.
17. Dong Z., Yang P., Li Q., Zhang M., Chang Y., Wang S. Fractional order modelling and optimal control of dual active bridge converters. *Systems Science & Control Engineering*, 2024, vol. 12, no. 1, art. no. 2347886. doi: https://doi.org/10.1080/21642583.2024.2347886.
18. Effah E.K., Anto E.K., Okyere P.Y., Effah F.B. Model Reference Adaptive Control of SPS-Based Dual Active Bridge Converter with Constant Power Loading. *Power Electronics and Drives*, 2024, vol. 9, no. 1, pp. 348-357. doi: https://doi.org/10.2478/pead-2024-0022.
19. Henao-Bravo E.E., Ramos-Paja C.A., Saavedra-Montes A.J., González-Montoya D., Sierra-Pérez J. Design Method of Dual Active Bridge Converters for Photovoltaic Systems with High Voltage Gain. *Energies*, 2020, vol. 13, no. 7, art. no. 1711. doi: https://doi.org/10.3390/en13071711.
20. Hessad M.A., Bouchama Z., Benaggoune S., Behih K. Cascade sliding mode maximum power point tracking controller for photovoltaic systems. *Electrical Engineering & Electromechanics*, 2023, no. 1, pp. 51-56. doi: https://doi.org/10.20998/2074-272X.2023.1.07.
21. Chen Q., Wang L., Sun Y., Xie S., Wang R. Adaptive integral sliding mode MPPT control for wind turbines with fixed-time convergence. *IET Renewable Power Generation*, 2024, vol. 18, no. S1, pp. 4265-4276. doi: https://doi.org/10.1049/rpg2.12935.
22. Bahri M., Talea M., Bahri H., Aboulfatah M. An efficient scanning algorithm for photovoltaic systems under partial shading. *International Journal of Electrical and Computer Engineering (IJECE)*, 2022, vol. 12, no. 6, pp. 5799-5807. doi: https://doi.org/10.11591/ijece.v12i6.pp5799-5807.
23. Bendib D., Laour M. Modified incremental conductance MPPT using SEPIC converter for PV system, simulation and Arduino implementation. *Studies in Engineering and Exact Sciences*, 2024, vol. 5, no. 2, art. no. e6614. doi: https://doi.org/10.54021/seesv5n2-090.
24. Benhacine T.Z., Dali A., Tata M., Kherbachi A., Boudraf M., Kaabeche A. Design of a test bench for a small wind turbine emulator. *Journal of Renewable Energies*, 2024, vol. 27, no. 1, pp. 5-13. doi: https://doi.org/10.54966/jreen.v27i1.1113.
25. Abo-Khalil A.G., Alobaid M. Optimized Control for PMSG Wind Turbine Systems under Unbalanced and Distorted Grid Voltage Scenarios. *Sustainability*, 2023, vol. 15, no. 12, art. no. 9552. doi: https://doi.org/10.3390/su15129552.
26. Ríos S.J., Pagano D.J., Lucas K.E. Bidirectional Power Sharing for DC Microgrid Enabled by Dual Active Bridge DC-DC Converter. *Energies*, 2021, vol. 14, no. 2, art. no. 404. doi: https://doi.org/10.3390/en14020404.
27. Sabhi K., Talea M., Bahri H. Improving Power Precision in Hybrid Renewable Energy Systems with a Quad Active Bridge DC-DC Converter and Neural Network-Based Decoupling. *2024 International Conference on Intelligent Systems and Computer Vision (ISCV)*, 2024, pp. 1-8. doi: https://doi.org/10.1109/ISCV60512.2024.10620155.
28. Mahamat C., Bechet J., Linguet L. Artificial Neural Network Control Applied to a Photovoltaic-Battery Microgrid System. *AI, Computer Science and Robotics Technology*, 2024, vol. 3, no. 1, pp. 1-20. doi: https://doi.org/10.5772/acrt.34.
29. Vamsi Krishna A., Sateesh B., Sai Sankar M., Sravanthi P., Vanaja Suvarna P., Devendra Goud E. A novel MPPT method for a standalone PV System. *International Journal for Modern Trends in Science and Technology*, 2024, vol. 10, no. 4, pp. 60-66. doi: https://doi.org/10.46501/IJMTST1004010.
30. Bana P.R., D'Arco S., Amin M. ANN-Based Robust Current Controller for Single-Stage Grid-Connected PV With Embedded Improved MPPT Scheme. *IEEE Access*, 2024, vol. 12, pp. 100251-100262. doi: https://doi.org/10.1109/ACCESS.2024.3429347.
31. Hichem L., Leila M., Amar O. The effectiveness of a hybrid MPPT controller based on an artificial neural network and fuzzy logic in low-light conditions. *Bulletin of Electrical Engineering and Informatics*, 2024, vol. 13, no. 3, pp. 1453-1464. doi: https://doi.org/10.11591/eei.v13i3.6416.
32. Costanzo L., Rubino G., Rubino L., Vitelli M. PFC Control Signal Driven MPPT Technique for Grid-Connected PV Systems. *IEEE Transactions on Power Electronics*, 2024, vol. 39, no. 8, pp. 10368-10379. doi: https://doi.org/10.1109/TPEL.2024.3393294.
33. Jasim A.M., Jasim B.H., Bureš V. A novel grid-connected microgrid energy management system with optimal sizing using hybrid grey wolf and cuckoo search optimization algorithm. *Frontiers in Energy Research*, 2022, vol. 10, art. no. 960141. doi: https://doi.org/10.3389/fenrg.2022.960141.

Received 23.08.2024
Accepted 19.11.2024
Published 02.03.2025

K. Sabhi[1], *PhD,*
M. Talea[1], *Professor,*
H. Bahri[1], *Professor,*
S. Dani[1], *PhD,*
[1] Department of Physics,
Hassan II University of Casablanca, Morocco,
e-mail: sabhi.khalid.imt@gmail.com (Corresponding Author);
taleamohamed@yahoo.fr; hbahri.inf@gmail.com;
said_dani@hotmail.fr

How to cite this article:
Sabhi K., Talea M., Bahri H., Dani S. Integrating dual active bridge DC-DC converters: a novel energy management approach for hybrid renewable energy systems. *Electrical Engineering & Electromechanics*, 2025, no. 2, pp. 39-47. doi: https://doi.org/10.20998/2074-272X.2025.2.06